Sixth International Symposium on Turbulence and Shear Flow Phenomena
Seoul, Korea, 22-24 June 2009

FRICTION DRAG REDUCTION THROUGH DAMPING OF THE NEAR-WALL SPANWISE VELOCITY FLUCTUATION

Bettina Frohnapfel
Center of Smart Interfaces, Technical University of Darmstadt
Petersenstr. 32, 64287 Darmstadt, Germany
frohnapfel@csi.tu-darmstadt.de

Yosuke Hasegawa, Nobuhide Kasagi
Department of Mechanical Engineering, The University of Tokyo
Hongo 7-3-1, Bunkyo-ku, Tokyo, 113-8656, Japan
hasegawa@thtlab.t.u-tokyo.ac.jp
kasagi@thtlab.t.u-tokyo.ac.jp

ABSTRACT

Direct numerical simulation (DNS) of a turbulent channel flow is performed in order to explore the possibility of reducing wall friction drag and saving energy through damping of the spanwise velocity fluctuation. Starting from an idealized feedback control, we extend the idea to a practically realizable control in which wall information is used as sensor input and actuators of finite size are employed. A novel control loop is proposed based on the upstream streamwise wall shear stress. This control scheme enables drag reduction of up to 20% while energy input for the control scheme remains two orders of magnitude smaller than the pumping power for the uncontrolled flow.

INTRODUCTION

Turbulence control techniques leading to skin friction drag reduction are of great economical and ecological interest. In general, active feedback control schemes offer potentially large energy gains that can be obtained with small power input. It is known that a feedback control, which introduces a spanwise damping force in the near-wall region, leads to drag reduction (Satake and Kasagi (SK), 1996 and Lee and Kim (LK), 2002). In the present work this "*w*-damping" is revisited to investigate the possibility of implementing it to a more realistic control scheme. Plasma actuators and Lorentz forces generally allow the introduction of tangential forces, but up to now no practical feedback scheme based on the *w*-damping concept is available.

PROCEDURE

We carry out DNS of a fully developed channel flow with a constant flow rate. The friction Reynolds number for the uncontrolled case is Re_τ=150. The present DNS is performed by a finite volume method on a staggered grid. The no-slip condition is imposed at the wall. For time advancement the Adams-Bashforth scheme is used for the convectional terms and the Crank-Nicolson scheme for the viscous terms. The computational domain is $2.5\pi \times 2\delta \times \pi\delta$ in x_1-, x_2- and x_3-directions, where δ is the channel half width. All simulations are carried out with 64x128x64 grid points. We have confirmed that doubling the grid number does not significantly affect the results shown in this paper.

A non-uniform mesh with a hyperbolic tangent distribution is employed in the x_2-direction resulting in a minimum grid size in wall-normal direction of $\Delta x_2^+{}_{min}$=0.188. The computational time step is chosen as $0.03\ \nu/u_\tau$ and the initial condition is given by a fully-developed velocity field of a preceding channel flow DNS. We also verified the present results by repeating selected simulations with a pseudo-spectral method where Fourier transforms in the streamwise and spanwise directions and Chebshev polynomials in the wall normal direction are employed. The pseudo-spectral method is also used for calculations at higher Reynolds numbers of Re_τ=300 and 450 with the same grid resolution in the viscous length unit.

As a control input for damping the spanwise velocity fluctuation we consider a feedback body force, bf_3, which is introduced into the Navier-Stokes equations. The modified spanwise momentum equation thus reads:

$$\frac{\partial u_3^+}{\partial t^+} + u_j^+ \frac{\partial u_3^+}{\partial x_j^+} = -\frac{\partial p^+}{\partial x_3^+} + \frac{\partial^2 u_3^+}{\partial x_j^+ \partial x_j^+} + bf_3^+ \qquad (1)$$

where the subscript $(\,)^+$ indicates normalization with the kinematic viscosity, ν, and the wall shear velocity, u_τ, of the uncontrolled channel flow. The last term on the right hand side represents the damping force. For the idealized *w*-damping, this force is proportional to the instantaneous spanwise velocity:

$$bf_3^+ = -\frac{f\left(x_2^+\right)}{\Phi^+} u_3^+ \qquad (2)$$

The relaxation time constant, Φ^+, determines the strength of the forcing, and $f(x_2^+)$ is a step function which defines the damping layer on the top and bottom walls where the forcing is applied: $f(x_2^+ \le y_d^+) = 1$, $f(x_2^+ > y_d^+) = 0$. The control input can be varied by modifying the relaxation time constant Φ^+ and the damping layer thickness y_d^+.

First, the influence of the damping layer thickness is investigated with the virtual control loop given by equation (1). To evaluate the drag reducing performance of the

control loop, it is compared with the virtual feedback control system by Iwamoto et al. (2005), which suppresses all turbulence fluctuations in a thin region adjacent to the wall. This control scheme serves as a reference for the present investigation since the relaminarization in the damping layer represents an idealized feedback control.

Next, the sensing and actuation requirements of the control loop are significantly reduced such that the flow state is detected only at the wall with sensors and actuators of finite dimensions.

For active flow control techniques, the control performance with respect to energy savings is captured with different indices. For constant mass flow the pumping power, P, is given as a function of the average streamwise wall shear stress, $\overline{\tau_u}$, and the bulk flow velocity U_b:

$$P = 2\overline{\tau_u} U_b . \tag{3}$$

Therefore, the energy saving rate is equivalent to drag reduction, DR:

$$DR = 1 - \frac{\overline{\tau_u}}{(\overline{\tau_u})_0} = 1 - \frac{P}{P_0}, \tag{4}$$

where the index $(\,)_0$ corresponds to the uncontrolled flow. In the present case the additional power input due to the applied control is defined as:

$$P_{in} = \int_0^H \left| \underbrace{\frac{1}{T}\int_0^T bf_3 u_3 dt}_{P_3} \right| dy, \tag{5}$$

where H corresponds to the channel height. The net energy saving rate, S, is given by:

$$S = 1 - \frac{P + P_{in}}{P_0} = DR - \frac{P_{in}}{P_0} \tag{6}$$

and the gain (i.e. savings per control input) is defined as follows:

$$G = (P_0 - P)/P_{in}. \tag{7}$$

IDEAL W-DAMPING

Figure 1 shows the time trace of the friction coefficient, $c_f = \overline{\tau_u} / 0{,}5\rho U_b^2$, with a damping layer thickness of y_d^+=5 and different damping forces (defined by the inverse of the relaxation time constant Φ^+). In the case of weak damping, an increase in the damping force strength results in a monotonous decrease of the skin friction. For stronger forcing ($(\Phi^+)^{-1} > 2/3$), DR asymptotically converges to

$$DR = 1 - (c_f / c_{f,0}) \approx 29\%. \tag{8}$$

This result shows that damping of the spanwise velocity component in the absolute vicinity of the wall is sufficient to achieve substantial drag reduction. Even for a forcing layer thickness of y_d^+=2.5, drag reduction of almost 20% is possible. With increasing damping layer thickness, drag reduction increases up to y_d^+=30, where relaminarization of the flow field is observed.

Based on the FIK identity (Fukagata et al., 2002), Iwamoto et al. (2005) presented a theoretical correlation between drag reduction, the Reynolds number, Re_τ, of the uncontrolled flow and the relative thickness of the damping layer, y_d/δ, in which the flow is forced to be laminarized. The above value of DR=29% coincides with this estimation of drag reduction for total suppression of turbulence in a damping layer y_d^+=5 at Re_τ=150. The same agreement between strong damping of the spanwise velocity component and suppression of all velocity components is found for a variety of damping layer thicknesses.

Figure 2 shows the Reynolds stresses in the controlled flows with damping forces of $(\Phi^+)^{-1}$ =1/15 and 2/3, and a damping layer thickness of y_d^+=10. They are compared with the uncontrolled channel flow and the controlled flow simulated by Iwamoto et al. (2005). In these plots, all variables are normalized by the wall shear velocity of the corresponding flow. It can be seen that the active damping of the spanwise velocity fluctuation also induces damping of the wall-normal velocity component. For the case of strong damping, the spanwise and wall-normal Reynolds stresses coincide with the reference case of Iwamoto et al. (2005). The same holds for the Reynolds shear stress, $\overline{u_1 u_2}$. This fact suggests the theoretical drag reduction predicted by Iwamoto et al. (2005) should also hold for the present control. The drag reduction predicted in their study shows that drag reduction due to the suppression of $\overline{u_1 u_2}$ in the damping layer exhibits only a weak Reynolds number dependency. Therefore, it is expected that the present control scheme will also work at higher Reynolds numbers. We confirmed that this is the case for Reynolds numbers of Re_τ=300 and 450.

A difference between the present control and suppression of all three velocity components appears in the streamwise velocity fluctuation. A reduction of the corresponding Reynolds stress, $\overline{u_1 u_1}$, in the near-wall region can be observed, but it remains significantly higher than $\overline{u_1 u_1}$ of the reference case. This is in agreement with the results of SK and LK. Therefore, the turbulent kinetic energy that remains in the flow field is higher in the present control than in the reference case of total damping. Since the same amount of drag reduction is achieved, this indicates that high net energy saving rates are possible.

Figure 3 shows the time trace of the average power input, P_{in}, for the current idealized feedback control in relation to the pumping power for the uncontrolled flow case, P_0. It can be seen that P_{in}/P_0 decays within t^+=100 from the initial values of 2% or 20%, respectively (depending on the strength of the forcing) to values below 1% indicating high S and G values.

In the idealized feedback loop, instantaneous velocity information and local introduction of a body force at every location in the damping layer is required. Since this assumption is unrealistic, it is desirable to develop a control algorithm with finite number of arrayed sensors and actuators placed on the channel walls

CLOSED LOOP CONTROL BASED ON THE STREAMWISE WALL SHEAR STRESS

The instantaneous spanwise wall shear stress, $\tau_w = (\partial u_3^+ / \partial x_2^+)_{wall}$, is well known to be useful for state estimation of wall turbulence and LK demonstrated that it is

also an appropriate sensor control input for *w*-damping with continuous sensing and actuation. However, it is difficult to measure τ_w in practice (Suzuki and Kasagi, 1992). Therefore, we focus on the streamwise wall shear stress, $\tau_u = (\partial u_1^+ / \partial x_2^+)_{wall}$, which can reliably be measured on a channel wall, as sensing quantity.

The instantaneous streamwise wall shear stress is strongly influenced by the presence of near-wall streaks. From the regeneration cycle of near-wall turbulence (Hamilton et al. 1995) it is known that near-wall streaks are not simply caused by the streamwise vortices, but that the breakdown of streaks will in turn lead to regeneration of the streamwise vortices. Underneath a streamwise vortex significantly large spanwise velocity fluctuations are induced. Therefore, the knowledge of the location and swirl direction of a streamwise vortex would enable the required damping of the spanwise velocity fluctuation.

Typical near-wall streaks are characterized by a spanwise gradient of the streamwise wall shear stress, τ_u, due the fact that low and high speed streaks occur in pairs. Therefore, we investigate the streamwise correlation between $\partial\tau_u / \partial x_3$ and the streamwise vorticity at x_2^+=15. The correlation is plotted as the solid line in figure 4. It can clearly be seen that the strongest correlation of almost 50% is located about 50 viscous length units downstream of the sensing location. This finding is in agreement with the results of Endo et al. (2002), who employed conditional averaging to investigate the spatial relation between streamwise vortices and meandering near-wall streaks.

Figure 5 shows the conditionally averaged flow field at Δx_1^+=50 downstream of the sensing location, given by $\partial\tau_u / \partial x_3 > 1.5(\partial\tau_u / \partial x_3)_{rms}$. A streamwise vortex with clockwise rotation is located at this position. The analysis of different downstream locations in the conditionally averaged flow field reveals that a streamwise vortex which is tilted away from the wall exists downstream of the sensing location. Based on the obtained results we propose an acuator input that depends on the upstream spanwise gradient of the streamwise wall shear stress, $\partial\tau_u / \partial x_3$.

In general, body forces can be introduced through Lorentz forces in electrically conducting fluids or through plasma actuators in air. These forces will decay from a maximum value at the wall. In order to mimic such a body force distribution, bf_3 is assumed to decay linearly from a finite value at the wall (determined by $(\Phi^+)^{-1}$) to zero at the edge of the forcing layer ($x_2^+=y_d^+$). In the present investigation the forcing layer thickness is fixed to y_d^+=10. The resulting body force thus reads:

$$bf_3^+ = (x_1^+, x_2^+, x_3^+) = -\frac{f(x_2^+)}{\Phi^+}(y_d^+ - x_2^+) \times \frac{\partial \tau_u^+}{\partial x_3^+}(x_1^+ - \Delta x_1^+, x_3^+) \qquad (9)$$

The dotted line in figure 4 shows the correlation between $\partial\tau_u / \partial x_3$ and the streamwise vorticity at x_2^+=15 for the controlled flow according to equation (9) when *DR* = 16.3%. While the value of the correlation is slightly reduced, the position of the strongest correlation remains at the same streamwise distance as for the uncontrolled flow. This result suggests that the upstream sensing of $\partial\tau_u / \partial x_3$ can also be applied in controlled flows to detect the existence and rotational direction of streamwise vortices.

The effect of the forcing strength, $(\Phi^+)^{-1}$, on the net energy saving rate, *S*, and energy gain, *G*, is shown in figure 6. Due to the large gain in the present control, *DR* and *S* are almost identical. With increasing forcing strength, *S* increases and then saturates while *G* increases and then decreases rapidly. This effect can be explained by investigating the details of the energy input.

The energy input as defined by equation (4) is given by the product of the body force, bf_3, and the spanwise velocity fluctuation, u_3. Therefore, the local energy input, P_3, is negative if the body force acts as a damping force and positive if it acts as a *w*-enhancing force. Figure 7 depicts the local energy input due to the applied body force as a function of wall distance for the same control settings as discussed in figure 6. For small forcing strengths, the body force acts as a damping force in the entire damping layer. For stronger forcing, positive values of P_3 can be found in the vicinity of the wall while P_3 is negative in the outer region of the damping layer. This indicates that bf_3 which decays linearly with distance from the wall is so strong in the vicinity of the wall that the spanwise velocity fluctuation is not only damped but forced to change its sign. It is noted that with further increase of the forcing strength, the simulation could not be continued.

In the case of weak forcing, the turbulence statistics are very similar to the ideal *w*-damping case shown in figure 2. Figure 8 shows the Reynolds stresses for a close loop control with strong forcing in comparison to those in the uncontrolled channel flow. It reveals that the spanwise velocity fluctuation is increased in the absolute vicinity of the wall and decreased at the outer edge of the damping layer. As observed in the ideal *w*-damping control, the wall-normal velocity component behaves similarly to the spanwise one, and also increases in the very near-wall region. Despite this increase, $-\overline{u_1 u_2}$, which determines *DR* (Fukagata et al. 2002), is reduced within the entire damping layer and has the same distribution as in the ideal *w*-damping case for the same drag reduction (not shown here). This behaviour can be attributed to reduction of $\overline{u_1 u_1}$ and decrease of the correlation coefficient within y_d^+.

A typical streamwise vortex in the flow field with strong forcing, $(\Phi^+)^{-1}$=0.94, is visualized in the bottom right corner of figure 8. It can be seen that the flow direction underneath the vortex has been changed in the near-wall region. This reverse flow seems to consume a lot of energy and thus lead to a significant reduction in the energy gain. Therefore, there exists an optimal strength, $(\Phi^+)^{-1}$, of the body force with respect to the energy gain. This is of major importance for the discussion of a possible practical realization of the proposed control loop since the efficiency of the actuator needs to be multiplied with the energy gain to obtain the efficiency of the total system.

Figure 9 shows a visualization of the controlled flow field in comparison to an uncontrolled flow. In the controlled flow the number of streamwise vortices is significantly reduced. The grey shading indicates the streamwise velocity at x_2^+=5. It reveals that the streamwise streaks in the near-wall region are weakened, elongated and spaced apart wider in the controlled flow.

EFFECT OF FINITE ACTUATOR SIZE

In order to further develop the control scheme towards a realistic system, the effect of finite actuator size needs to be taken into account. The correlation displayed in figure 5 suggests that drag reduction can be obtained for a range of distances between sensor and actuator, Δx_1^+. Therefore, a parametric study is performed, and the influence of Δx_1^+ on the drag reduction performance is investigated. Simulations are repeated for the four different forcing strengths displayed in figure 7. For the two stronger forcing cases, which are characterized by positive values of P_3 in the near wall region, the simulation became unstable with increasing Δx_1^+. For $(\Phi^+)^{-1}$=0.24 and 0.12, all simulations converged. In these simulations the local energy input, P_3, assumed negative values throughout the entire forcing layer, indicating that the applied force acted as a damping force.

Figure 10 shows the influence of a modified Δx_1^+ on the energy saving rate for $(\Phi^+)^{-1}$=0.24. It can be seen that an almost constant value of $S \approx 17\%$ is obtained over a wide range. The maximum value of S =17.6% is located at Δx_1^+=84, which corresponds to $\Delta x_1'$=76 if normalized with the inner variables of the controlled flow. This value differs from the location of the highest correlation displayed in figure 4 indicating that the streamwise vorticity at x_2^+=15 might not be the best indicator for the optimum actuator placement. The conditionally averaged flow field reveals that at Δx_1^+=84 the flow field is not so much characterized by a streamwise vortex anymore but only by a strong spanwise motion in the near-wall region.

Therefore, we focus on the spatial correlation between $\partial \tau_u / \partial x_3$ and the spanwise wall shear stress, τ_w. Figure 11 shows the results obtained for channel flows at different Reynolds numbers. The location of the strongest correlation for Re_τ=150 shows good agreement with the location for which the maximum drag reduction was detected in the controlled flow suggesting that the correlation with τ_w is a good indication for the optimum actuator placement. At Re_τ=300 and 450 the maximum correlation coefficient is reduced and shifted to slightly smaller Δx_1. However, the difference between Re_τ=300 and 450 is small, suggesting that, at higher Reynolds numbers, the Reynolds number influence will be small and that the optimum actuator placement will be located around Δx_1^+=40.

To investigate the influence of finite size actuators, a finite streamwise length of the actuators is introduced instead of continuous actuation along the channel walls. The information of only one upstream sensor is thus used for a number of consecutive downstream locations. Since the maximum net energy savings rate was obtained for Δx^+=84, the actuator center is placed at this location. Actuator lengths of 37, 75 and 150 viscous units were tested. These configurations result in S = 18.5%, 18.5% and 18.2%, respectively suggesting that the actuator can be designed with a streamwise extension of 100 viscous length units and even more. Investigations on the influence of the spanwise extension of the actuator reveal that increased spanwise dimensions lead to a reduction of the net energy savings.

For all present results, the energy saving due to the applied control is at least two orders of magnitude larger than the energy input, i.e. G >100.

CONCLUSION AND OUTLOOK

The present investigation demonstrates that strong *w*-damping enables the same drag reduction as the total suppression of all velocity fluctuations in the near-wall region. Therefore, we may expect that flow control techniques based on *w*-damping will also work at high Reynolds numbers and first simulations at Re_τ=300 and 450 confirm this expectation.

A novel control loop which is designed to damp the spanwise velocity fluctuations in the downstream near-wall region is proposed. The sensor input is given by the spanwise gradient of the streamwise wall shear stress, $\partial \tau_u / \partial x_3$, up to 150 viscous units upstream of the actuator. This control loop is considered to be of practical importance, because the streamwise wall shear stress is easier to measure than the spanwise one and also the sensor placement in a range of upstream locations is possible. The latter enables the use of actuators with large streamwise extension. While the streamwise extension of the actuators is found to have a weak, even slightly positive, influence on drag reduction, the spanwise extension seems to have stronger limitations. An important feature of the proposed control loop is the high energy gain which can be optimized based on the control strength.

Future work will address the question of how to estimate this optimal forcing strength beforehand and investigate the influence of streamwise and spanwise separation of the actuators as well as the Reynolds number dependency.

ACKNOWLEDGMENTS

BF wishes to gratefully acknowledge the support of the Japan Society for the Promotion of Science (JSPS) during her stay at the University of Tokyo.

REFERENCES

Endo, T., Kasagi, N., Suzuki, Y., 2000, "Feedback control of wall turbulence with wall deformation", *Int. J. Heat & Fluid Flow*, Vol. 21, pp. 568-575.

Fukagata, K., Iwamoto, K. and Kasagi, N., 2002, "Contribution of Reynolds stress distribution to the skin friction in wall-bounded flows" *Phys. Fluids*, Vol. 14, pp. L73-L76.

Hamilton, J.M., Kim, J., Waleffe, F., 1995, "Regeneration mechanism of near-wall turbulence structures", *J. Fluid Mech.*, Vol. 287, pp. 317-348.

Iwamoto, K., Fukagata, K., Kasagi, N., Suzuki, Y., 2005, "Friction drag reduction achievable by near-wall turbulence manipulation at high Reynolds number" *Phys. Fluids*, Vol. 17, Art. No. 011702.

Lee, C., Kim, J. 2002 "Control of the viscous sublayer for drag reduction", *Phys. Fluids*, Vol. 14, pp. 2523-2529.

Satake, S., Kasagi, N. 1996 "Turbulence control with wall-adjacent thin layer damping spanwise velocity fluctuations", *Int. J. Heat Fluid Flow*, Vol. 17, pp. 343-352.

Suzuki, Y., Kasagi. 1992 "Evaluation of hot-wire measurement in wall shear turbulence using a direct numerical simulation database", *Experimental Thermal and Fluid Science.* Vol. 5, pp. 69-77.

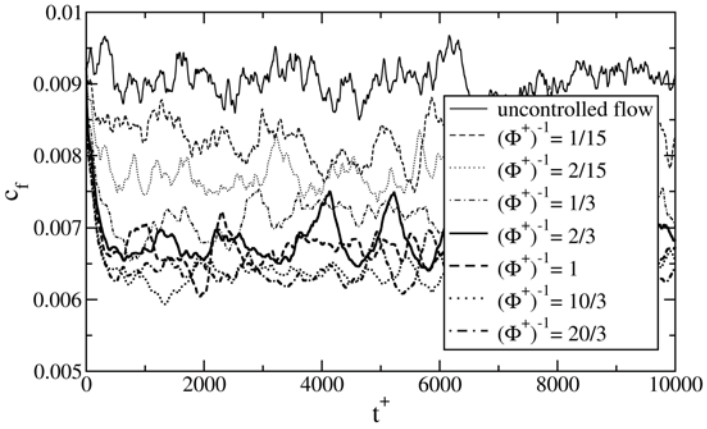

Figure 1: Time traces of the c_f-value for a channel flow with a forcing layer thickness of y_d^+=5.

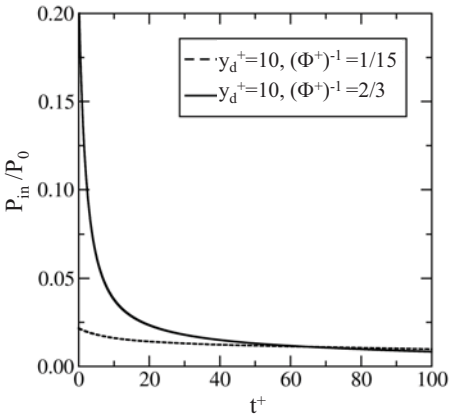

Figure 3: Time trace of the control energy input, P_{in}, normalized by the pumping power of the uncontrolled channel flow W_0.

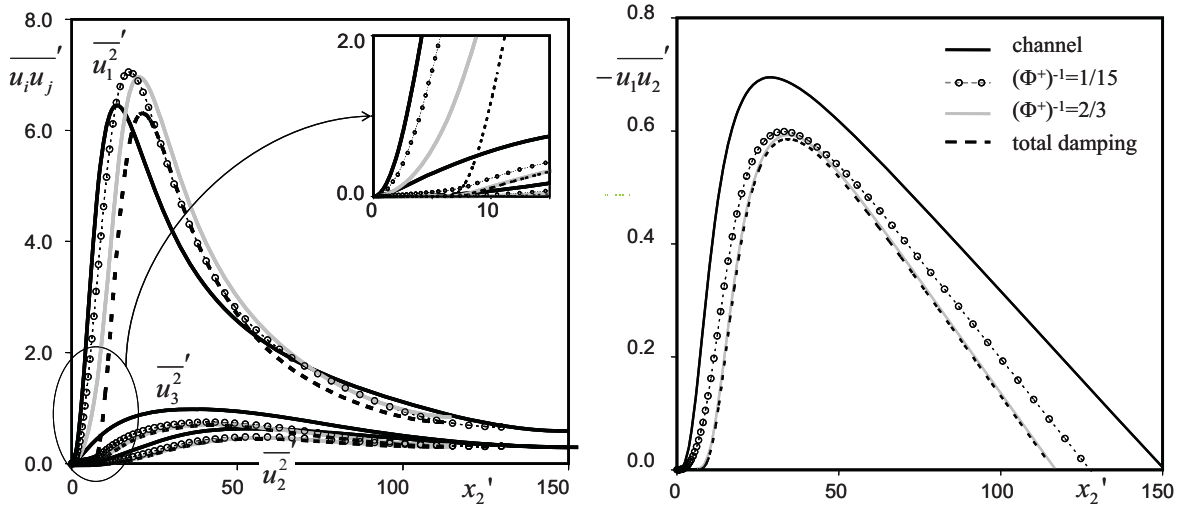

Figure 2: Reynolds stresses of controlled flows (y_d^+=10) in comparison with the Reynolds stresses of the uncontrolled channel flow and of the total damping case (Iwamoto et al., 2005). The dash indicates that the normalization is based on the inner variables of each controlled flow.

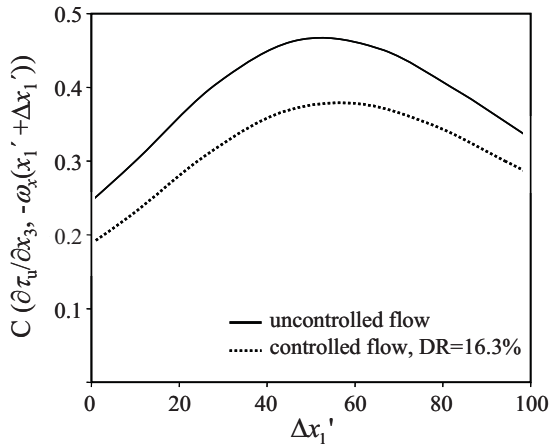

Figure 4: Spatial correlation, C, between the spanwise gradient of the streamwise wall shear stress and the streamwise vorticity at different downstream locations for an uncontrolled flow and a controlled flow according to equation (9). The normalization is based on the inner variables of each flow.

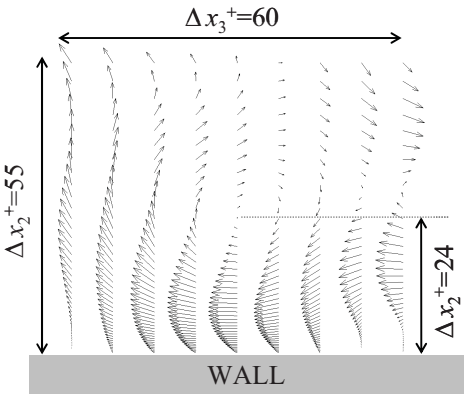

Figure 5: Conditionally sampled flow field at Δx_1^+=50 behind the measuring location.

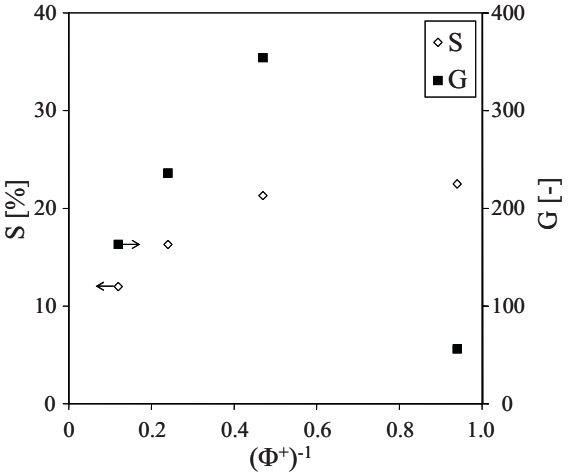

Figure 6: Effect of the forcing strength $(\Phi^+)^{-1}$ on S and G for flow the flow control loop given by equation (9).

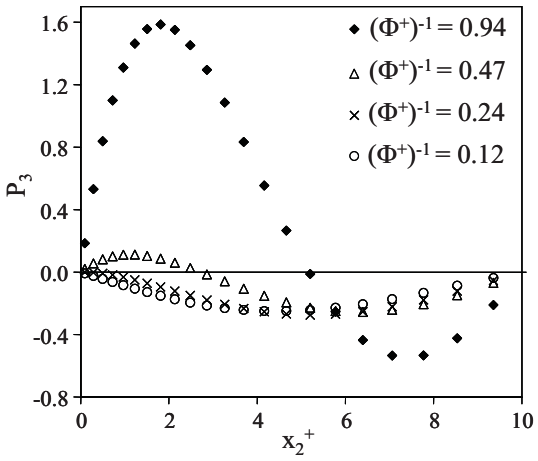

Figure 7: Local energy input, P_3, as a function of wall distance for different forcing strengths.

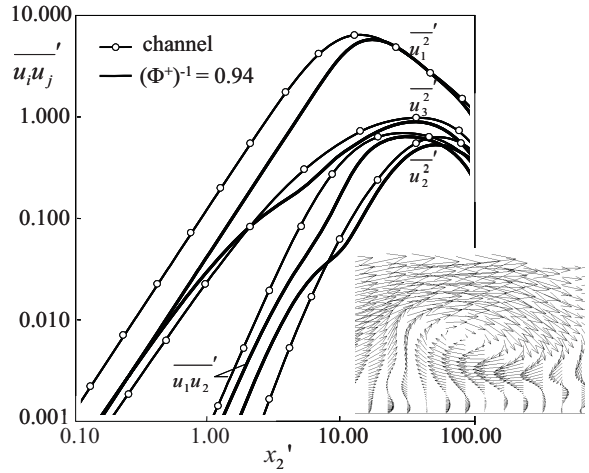

Figure 8: Reynolds stresses for a controlled flow according to equation (9) in comparison to an uncontrolled channel flow and a typical streamwise vortex of the controlled flow field. In case of the controlled flow the normalization is based on the respective inner variables.

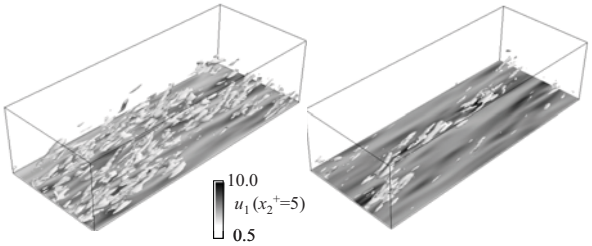

Figure 9: Flow visualization of the uncontrolled channel flow at Re_τ=150 (left) and the controlled case (S=17.6%) according to equation 9 (right). The visualization of the streamwise vortices is based on isosurfaces for which the second invariant of the deformation tensor is given by II^+=0.02.

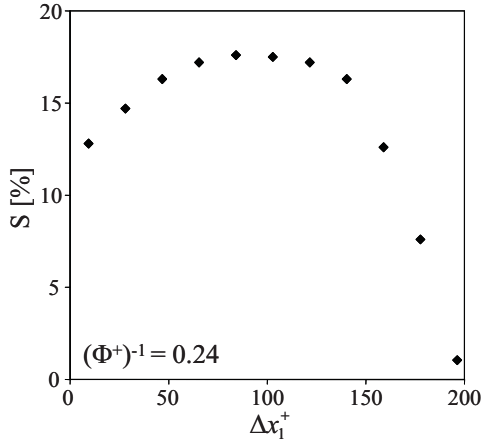

Figure 10: Influence of the streamwise distance, Δx_1^+, between sensor and actuator on the net energy saving rate, S.

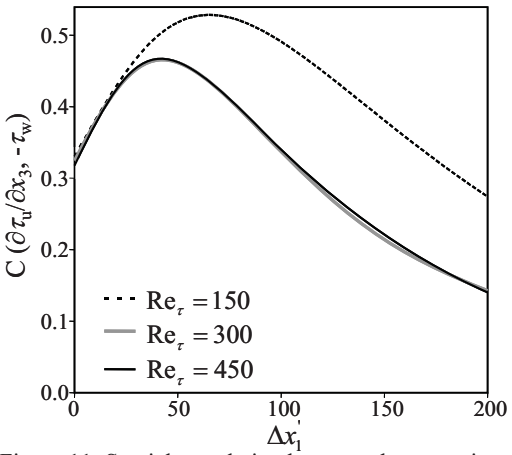

Figure 11: Spatial correlation between the spanwise gradient of the streamwise wall shear stress and the negative spanwise wall shear stress at different Reynolds numbers.